Red luminescence and UV light generation of europium doped zinc oxide thin films for optoelectronic applications

Mohamed El Jouad, El Mehdi Bouabdalli, Samira Touhtouh, Mohammed Addou, Nadège Ollier, Bouchta Sahraoui

Eur. Phys. J. Appl. Phys. **91**, 10501 (2020)

https://doi.org/10.1051/epjap/2020200133

THE EUROPEAN PHYSICAL JOURNAL APPLIED PHYSICS

Regular Article

Red luminescence and UV light generation of europium doped zinc oxide thin films for optoelectronic applications

Mohamed El Jouad[1,*], El Mehdi Bouabdalli[1], Samira Touhtouh[1], Mohammed Addou[2], Nadège Ollier[3], and Bouchta Sahraoui[4]

[1] The Engineering Sciences Laboratory for Energy, National Engineering School of Applied Sciences. Chouaib Doukkali University, El Jadida, Morocco
[2] Laboratory of Materials and Valorizations of Natural Resources, University Abdelmalek, Essaadi, Tangier, Morocco
[3] Laboratoire des Solides Irradiés (LSI), CEA/DRF/lRAMIS, Ecole Polytechnique, CNRS, lnstitut Polytechnique de Paris, 91128 Palaiseau, France
[4] Institute of sciences and molecular technologies of Angers, MOLTECH Anjou − UMR CNRS 6200 Molecular Interaction Nonlinear Optics and Structuring MINOS, 49045, ANGERS cedex 2, France

Received: 11 May 2020 / Received in final form: 15 June 2020 / Accepted: 19 June 2020

Abstract. In the present work, the Europium doped Zinc Oxide (ZnO: Eu) thin films were elaborated using spray pyrolysis technique. We are interested in investigating the structural properties, photoluminescence (PL) and third harmonic generation (THG) of the elaborated films. The structural properties of as-prepared thin films were characterized by X-ray diffraction (XRD). It confirms that all deposited thin films of Europium doped Zinc Oxide are crystallized in the hexagonal wurtzite structure. Both undoped and doped europium thin films show strong preferred c-axis orientation. Photoluminescence (PL) emission from Europium doped Zinc Oxide thin films, under excitation by 266 nm, shows characteristic transitions of Europium ($^5D_0 \rightarrow {}^7F_0$, $^5D_0 \rightarrow {}^7F_1$, $^5D_0 \rightarrow {}^7F_2$, etc.). It reveals the good incorporation of Eu^{3+} ions in the ZnO host. Additionally, the $^5D_0 \rightarrow {}^7F_2$ is the most intense transition usually observed for Eu^{3+} embedded in materials of Zinc Oxide lattice. The dependence of third-order nonlinear susceptibility on doping rate was evaluated. The highest nonlinear susceptibility χ^3 is obtained for the 5% Europium doped ZnO sample.

1 Introduction

Wide band gap semiconductors have attracted particular interest for applications in semiconductor electronics as well as electro-optical and nonlinear optics devices. The zinc oxide (ZnO) is characterised by an optical transition in the near ultraviolet (UV) (gap = 3.37 eV) and its large exciton binding energy of 60 meV [1]. The areas of interest to materials based on ZnO and related heterostructures are highly demanded for technological applications, especially for the use in various electronic, optoelectronics devices, spin electronics and microelectronics, such as gas sensing applications, surface acoustic wave devices, transparent coating and solar cell applications [2], especially in the form of nanoparticles. Many investigations on structural, electrical and optical properties of undoped and doped ZnO were carried out [3–10]. The electronic and optical properties of ZnO are profoundly modified and depend on the size, form and surface state of the nanocrystals. The interest is to control these parameters to adjust the desired properties. However, its fast recombination of generated electron-hole pairs limits its usefulness. This latter can be resolved by rare earth ions doping. This also makes it possible to increase the lifetime of charge carriers and subsequently reduce the probability of recombination [11]. Rare earth (RE) ion doped ZnO semiconductors have generated a great interest, compared to 3d transitions metal and non-metal transitions doping, because they are characterized by, on the one hand, their $f \rightarrow f$ or $f \rightarrow d$ internal orbital transitions give very intense and narrow emission lines in the ultraviolet (UV), visible and infrared regions [12,13]. On the other hand, they are characterised by long energy levels lifetimes that reach milliseconds (ms). However, the problem with rare earth doped ZnO is that the luminescence of the rare earth centers is weaker than that of the excitons and defects originating from ZnO. There are several techniques for showing rare earth emissions at the expense of the intrinsic luminescence of ZnO by optimizing the deposition conditions or by doping with coactivators such as lithium ions, nitrogen. In this study, we will be interested by europium ions doping. On the one hand, the europium ion is used because it is known to be the most sensitive probe, among rare earths, for the structure and symmetry of its environment [14–18]. Thus, it allows a better understanding of the distribution of environments within occupied sites. On the other hand, this ion is used mainly for its red emission located around 615 nm. This ion is an important candidate for doping ZnO [19–26], due to its possible application in the optoelectronics field, which attracts research groups. Though, the pure and narrow red broadcast could not be obtained, because

* e-mail: eljouad.m@ucd.ac.ma

the latter is always accompanied by a large green emission from the auto-activation centers. It is well known that zinc oxide easily produces intrinsic defects such as interstitial zinc (Zni**) and oxygen vacancies (Vo**). Several other attempts were made to obtain a strong red luminescence of ZnO: Eu, in particular the role of the solvent and of the temperature treatment in the luminescence behaviour of ZnO: Eu^{3+}. In the literature, the thin films of undoped and Eu-doped ZnO are prepared by numerous methods: chemical vapor deposition (CVD) [27], Pulsed Laser deposition [28], hydrothermal method [29], RF magnetron sputtering [30]. These techniques lead to the production of high films quality, however they are expensive (purchase + maintenance). Hence the orientations towards less expensive investment techniques like the sol-gel method [31], electrochemistry [32] or even synthesis by "spray pyrolysis" [33–35]. These methods are easier to implement and lead to good quality materials. In our case, we will only be interested in the last technique which is the reactive chemical spraying in liquid phase "Spray pyrolysis" which is characterized by its simplicity of implementation, its low cost and also it remains attractive for the depositing films with good uniformity over a large area. This deposition technique takes its principle from Chamberlin, the first who discovered it in 1966 [36]. It consists in spraying fine droplets, on a previously heated substrate, a generally aqueous solution containing atoms of the chosen compound. The salts used in this deposition process are often chlorides, both for the base oxide and for the dopant. Under the effect of temperature, there is indeed a reaction and therefore formation of the film on the substrate. One of the advantages of the used technique in this work is the choice of the starting solution. Indeed, we opted for solutions of chlorides dissolved in water. The films prepared from chlorides presents better luminescence intensity and good cristallinity related to a dense structure and crystallites size relatively important [37], which confirms our choice for this precursor. The use of this solvent reduces the quantity of precursors used and avoids the toxicity and corrosion problems encountered in the preparation of these layers by reactive chemical spraying. The objective of this article is to contribute to the development of thin layers of europium doped ZnO in order to control and improve the properties of Solar cells (Down-converter layer), optoelectronic components such as LEDs, electro-optical and non-linear optical devices. In this study, Europium doped Zinc Oxide were elaborated using spray pyrolysis technique. The structural, linear and nonlinear optical properties were investigated. We present the energy transfer process from ZnO host to Eu^{3+} ions and we suggest a suitable mechanism for the energy transfer process. In addition, we analysed the effect of Eu^{3+} doping on the third order nonlinear optical susceptibility.

2 Experimental details

The schematic set-up for the thin film elaboration used in our laboratory is shown in Figure 1. Europium doped Zinc oxide thin films were prepared from a solution of zinc chloride ($ZnCl_2$; Sigma-Aldrich 99,99%) and europium

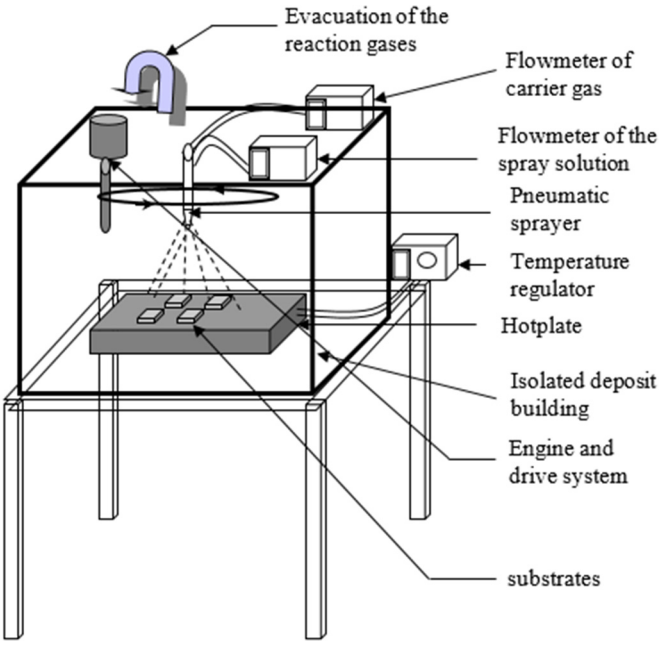

Fig. 1. Diagram of the spray pyrolysis device.

Chloride ($EuCl_3$,$6H_2O$; Sigma-Aldrich 99.99%) dissolved in deionised water and transported in tubes using a pump flow meter to regulate the spray rate of the solution (4 ml/min), which is sprayed in fine droplets using air as a carrier gas. The nozzle is directed towards the substrate (distance nozzle-substrates 40.5 cm). This solution was sprayed, during 4 min, onto clean glass substrates with a size of (25 mm × 25 mm × 1 mm) heated at 450 °C by a ceramic heater. The atomic concentration of Eu in the solution was varied from 1 to 5 at.%. After deposition, the films were cooled to room temperature.

The structural analysis of obtained thin films was carried out using X-ray diffraction (monochromatic Cu kα radiation $\lambda = 0.15405$ nm) and profilometry. The emission spectra were acquired at ambient temperature using an ANDOR Shamrock spectrometer associated with an intensified IStar CCD camera. The laser used for excitation is a pulsed laser Nd: YAG Quanta ray INDI 40–10 emitting at three different wavelengths: 532 nm, 355 nm and 266 nm. This latter is used to excite the sample in our case. The axis of the optical fiber collecting the light emitted by the sample makes an angle of 90° with the axis of the laser beam. Third order nonlinear optical susceptibilities χ^3 of undoped and doped ZnO thin films were examined by the THG method [38]. The experimental arrangement that we used for the measurements of the generation of the third harmonic, represented on the Figure 2, uses a laser of the type (Q-switched mode-locked Nd: YAG) whose fundamental beam has a wavelength of 1064 nm, it is a model (Quantum elite). For a 15 ps pulse it delivers an energy of 1.6 mJ, the frequency of which is 10 Hz. The energy and polarization of the fundamental beam are controlled by a half-wave plate located between two polarisers. Part of the incident beam was selected and measured by a photodiode helping to monitor the incident energy. Then the beam is focused on the sample using a lens with focal length of

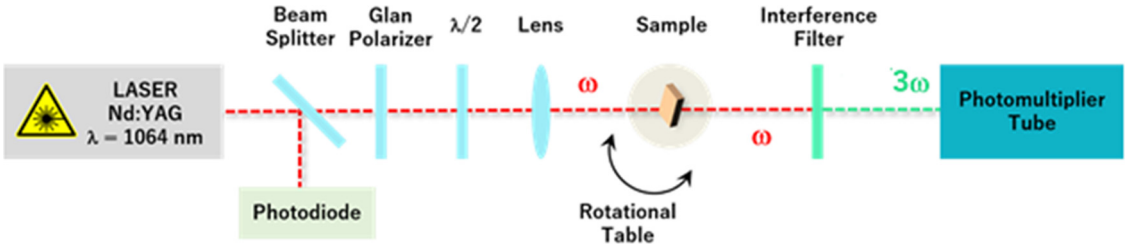

Fig. 2. THG experimental setup.

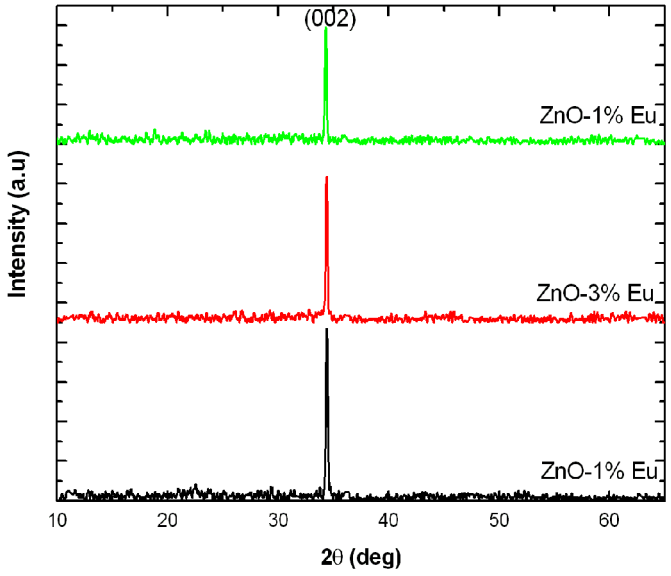

Fig 3. X-ray diffraction patterns of Eu-doped ZnO thin films with different Eu concentrations (1%, 3%, 5%).

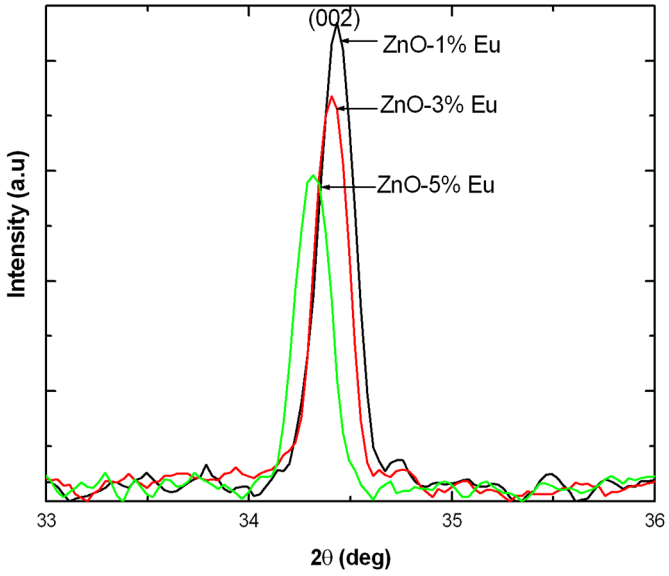

Fig. 4. Presents a displacement Δ ($2\theta_{002}$) in the position of the diffraction peak (002) of the Eu-doped ZnO thin films as function of diffraction angle.

25 cm. The surface excited by the beam has a diameter of 0.65 mm, the energy density applied is 2 GW/cm^2. The sample is mounted on a stepping motor (turntable). A filter was used to screen the fundamental beam at 1064 nm and then a selective filter (at 355 nm) allowing only the generated beam to be collected in a tube photomultiplier (PMT). We also used density filters to reduce the intensity produced by the non-linear medium. The signal for the third harmonic was detected by a PMT (model: Hamamatsu), integrated with a boxcar and processed by a computer. This produces the Maker fringes, which were produced by rotating the sample around an axis ranging from the angle (−60°) to (+60°).

3 Results and discussion

Figure 3 shows the XRD patterns of ZnO: Eu^{3+} thin films (deposited on glass substrates) prepared by spray pyrolysis method. It shows that the layers are well crystallized in the hexagonal wurtzite structure with the same preferential orientation. The strongest diffraction peak, corresponding to the (002) crystal plane of Eu doped ZnO, revealed the preferred orientation along the c-axis of ZnO crystals. Which correspond to the lowest surface energy for the wurtzite structure of ZnO. Also, it is noted that the XRD peaks are very narrow showing a good crystallinity of the prepared thin films. No extra peaks associated to dieuropium trioxide or any other incidental impurities were detected. This indicated that the pure phase of ZnO wurtzite structure was crystallized. This proves that the Eu^{3+} ions have very well incorporated in the ZnO lattice. It is clear that incorporation of Eu^{3+} ions with bigger ionic radius (0.95 Å) to the ZnO host with smaller zinc ionic radius (0.74 Å) deteriorated the film's crystallinity. From Figure 3, we have observed that the intensity of the preferential plane peak (002) of thin films of Eu-doped ZnO decreases as the doping level of europium increases from 1% to 5%. This is related to the influence of various factors such as the spray temperature, flow rate of the sprayed solution and spontaneous cooling. In this case, it may happen that the crystallites are oriented, not completely random, but preferably in one or more particular directions [39]. The X-ray diffraction peaks of Eu-doped ZnO thin films shifts slightly towards small when the europium doping rates increases from 1% to 5% as shown in Figure 4. The position of the diffraction peak (002) of the Eu-doped ZnO thin films decreases from 34,433° for an Eu at 1% doped ZnO thin film to 34,316° for Eu at 5% doped ZnO. This peak displacement results from the structural strain associated with Eu doping, determined using the following

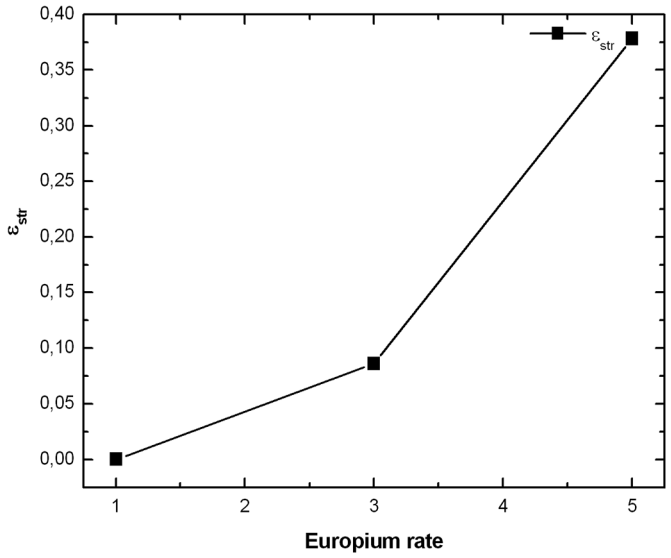

Fig. 5. Structural strain of Eu-doped ZnO thin films as function the europium concentration.

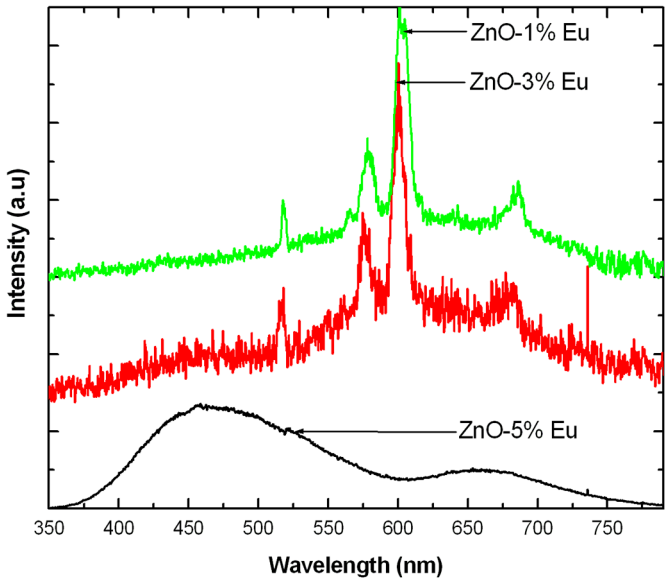

Fig. 6. Room temperature photoluminescence (PL) emission spectra of the Eu-doped ZnO with different Eu concentration (1%, 3%, 5%).

Table 1. Lattice parameters of the undoped and Eu doped ZnO thin films.

Sample	c (A)	a (A)	Volume (A^3)	c/a
ZnO	5190	3238	47 125	1603
ZnO : 1% Eu	5204	3261	47 926	1596
ZnO : 3% Eu	5210	3271	48 279	1593
ZnO : 5% Eu	5222	3283	48 743	1591

relation [40]:

$$\varepsilon_{\mathrm{str}} = -\Delta\theta_{\mathrm{hkl}} \frac{1}{tg(\theta_{\mathrm{hkl}})} \quad (1)$$

where $\varepsilon_{\mathrm{str}}$ is structural strain; $\Delta\theta_{\mathrm{hkl}}$ is the width at half height expressed in radian (it's calculated compared to ZnO-1% Eu taken as origin); θ_{hkl} is the diffraction angle.

Figure 5 also demonstrates that the structure strain varies from 0.00 to 0.38 for 1% Eu-doped ZnO towards 5% Eu-doped ZnO. This big increase in the value of the constraint is able to create a change in the structure, it can produce a slight increase in the lattice parameter (Tab. 1). The lattice parameter c value of Eu-doped ZnO thin films was calculated from X-ray diffraction pattern [41]. From calculated value of lattices parameters (Tab. 1), it is found that these parameters increase with the percentage of the concentration of europium (Eu) from 1% Eu to 5% Eu in the lattice ZnO. It can be explained by the cationic substitution of Eu^{3+} ions (ionic radius 0.95 Å) by Zn^{2+} ions (ionic radius 0.74 Å). Similar behaviour was detected for cerium and erbium doped ZnO thins films [42,43].

Figure 6 shows the photoluminescence spectra of the samples of 1%, 3% and 5% Europium doped ZnO excited at 266 nm. In order to be able to compare the different spectra, we normalized all of them on the maximum intensity of the transition $^5D_0$-$^7F_1$ because her intensity is not very

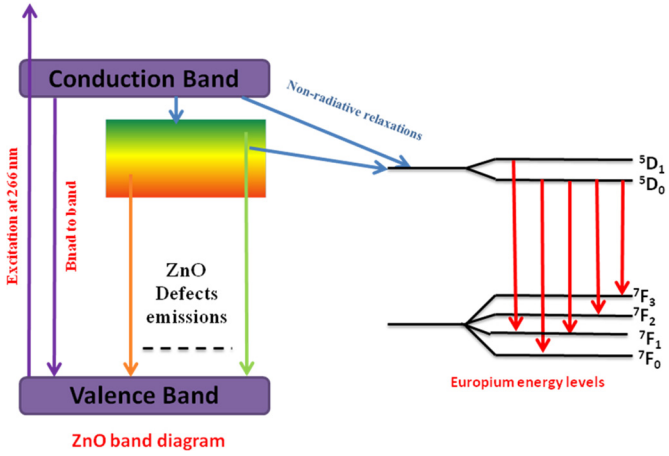

Fig. 7. Schematic band diagram illustrating the ZnO and Eu^{3+} ions emissions and the energy transfer mechanism between them.

sensitive to the environment around the Eu^{3+} rare earth ion. The photoluminescence spectrum of ZnO-1% Eu shows only broad bands characteristic of oxygen and zinc defects in interstitial sites [44–47]. However, in the case of the two other samples, in addition to the weak broad bands characteristic of ZnO, the spectra exhibit sharp peaks originating from the intra-4f transitions of the Eu^{3+} ions. This could be explained by the fact that after the ZnO band gap excitation, the relaxation of the carriers towards the band edge of the conduction band (CB) and the Valence band (BV) takes place, where they are quickly trapped at the level of the ZnO defects or give a Band edge radiative emission. This is explained by the fact that these carriers trapped in oxygen vacancies could transfer their energy to the Eu^{3+} ions via an energy transfer process. Similar energy transfer behaviour is observed in other studies [48–50]. Subsequently, we observe the radiative transitions from ^5D to ^7F as shown in Figure 7. The emissions observed at 517,

Table 2. Intensity ratio $^5D_0 \rightarrow {}^7F_2/{}^5D_0 \rightarrow {}^7F_1$ for Eu doped ZnO with different europium rates.

Samples	$^5D_0$-$^7F_2$/$^5D_0$-$^7F_1$
ZnO–1% Eu	–
ZnO–3% Eu	1.36
ZnO–5% Eu	1.27

560, 575, 600, 680 nm corresponding respectively to $^5D_1 \rightarrow {}^7F_1$, $^5D_0 \rightarrow {}^7F_0$, $^5D_0 \rightarrow {}^7F_1$, $^5D_0 \rightarrow {}^7F_2$ and $^5D_0 \rightarrow {}^7F_3$ europium transitions. The emission of level $^5D_1$ is a characteristic of a low phonon energy host. These phonons are responsible for the mechanism of non-radiative transitions between the energy levels of the rare earth. The dominant peak is observed at 600 nm due to the $^5D_0 \rightarrow {}^7F_2$ transition. The emission intensity increased with the increase in the concentration of Eu^{3+} till to 3%, and then it decreases. This can be explained by the phenomenon of extinction of the concentration [51] and the formation of Eu_2O_3 [50]. At a higher dopant concentration, the ability to form Eu_2O_3 is energetically more favorable.

Table 2 summarizes the relative intensities of the $^5D_0 \rightarrow {}^7F_2$ transition versus the $^5D_0 \rightarrow {}^7F_1$ transition for the two samples. Hypersensitive transitions (that obey the selection rules $|\Delta J| = 2$, $|\Delta L| \leq 2$ and $|\Delta S| = 0$) such as $^5D_0 \rightarrow {}^7F_2$ tend to be much more intense in non-symmetrical sites whereas the transition $^5D_0 \rightarrow {}^7F_1$ which is a magnetic dipole, its intensity is almost independent of local environment. This is why the intensity ratio $^5D_0 \rightarrow {}^7F_2/{}^5D_0 \rightarrow {}^7F_1$ is a good measure of the environmental symmetry of the rare earth ion. The ratio of intensities $^5D_0 \rightarrow {}^7F_2$ /$^5D_0 \rightarrow {}^7F_1$ is higher for ZnO-3% Eu sample, which indicates that the environmental symmetry of Eu^{3+} is slightly lower in the latter. From the results of photoluminescence it could be deduced that the thin layers of ZnO: Eu can be used in solar cells and light-emitting diodes as down-converter layer and emitting layer respectively.

Figure 8 gives the signal intensity for layers doped with 1%, 3% and 5%. Indeed, the signal intensity increases and adopts a bell shape with a slight appearance of the fringes. This form was explained by Castañeda et al [52], as being due to the thickness of the layers which is less than the coherence length of the oxide and which is of the order of 1 μm. This explanation does not seem very decisive, because our thin layers have the same thickness. The intrinsic zinc oxide is homopolar. So the introduction of the Eu^{3+} ion would probably lead to a substantial redistribution of the charge density as well as to an additional polarization by charge density which could improve the nonlinear optical properties.

This signal intensity affects the value of the nonlinear susceptibility. In Table 3, we group the calculated χ^3. For zinc oxide the susceptibility value is much higher than the value of the reference material. Europium introduces a redistribution of electronic charge density thus inducing a substantial polarization [53]. As expected there is an improvement in nonlinear properties and an increase in the susceptibility value. The systematic study according to the doping rate revealed that the best susceptibility value is obtained by doping with 5% europium. This makes this latter one of the good candidate materials for nonlinear optical device applications

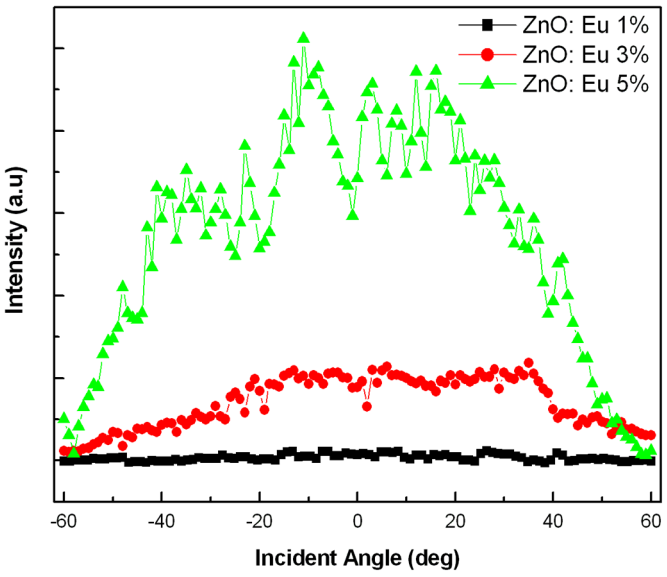

Fig. 8. Normalized third-harmonic response of Eu-doped ZnO thin films with different Eu concentrations (1%, 3%, 5%).

Table 3. Third order nonlinear susceptibility, and thickness of Eu doped ZnO with different europium rates.

Sample	Thickness (nm)	$(\chi^3 \pm 0.1)^* 10^{-12}$ (esu)
SiO2 reference material		0.026
ZnO	200	9280 [38]
ZnO: Eu 1%	200	7320
ZnO: Eu 3%	220	33 430
ZnO: Eu 5%	250	65 840

4 Conclusion

In summary, a simple, effective and economical method of production, of europium doped Zinc Oxide, based on the spray pyrolysis was proposed. The samples were characterized by photoluminescence using a 266 nm excitation. We have convincingly demonstrated that efficient energy transfer takes place from the ZnO host to Eu^{3+} ions. This energy transfer gave a strong red emission at 600 nm ($^5D_0 \rightarrow {}^7F_2$) of the Eu^{3+} ions. We have also shown that doping with europium improves significantly third-order nonlinear susceptibility. The highest susceptibility value is recorded for ZnO: 5% Eu ($65.840*10^{-12}$ (esu)). These results show that the thin layers of ZnO: Eu are good candidates in order to control and improve the properties red light sources, electro-optical, non-linear optical devices and solar cells

especially dye-sensitized solar cells (DSSC) to which we are going, in future, to incorporate the studied films in DSSC as a down-converter layer in order to enhance their efficiency.

This work is supported by CNRST, Hassan II Academy of Science and Technology, PPR/2015/9-Morocco. The corresponding author would like to express his deep gratitude to Professor Jean Michel Nunzi (Queen's University) for his support and his intellectual discussions on the subject which led to the generation of new ideas in this work.

Author contribution statement

All authors have contributed equally to this work.

References

1. B. Marí, M. Mollar, A. Mechkour, B. Hartiti, M. Perales, J. Cembrero, Microelectron. J **35**, 79 (2004)
2. R. Chander, A.K. Raychaudhuri, Solid State Commun. **145**, 81 (2008)
3. S.W. Chan, R.J. Barille, J.M. Nunzi, K.H. Tam, Y.H. Leung, W.K. Chan, A.B. Djurišić, Appl. Phys. B **84**, 351 (2006)
4. S.H. Mohamed, S.A. Ahmed, Eur. Phys. J. Appl. Phys. **44**, 137 (2008)
5. S. Bhatia, N. Verma, M. Aggarwal, Eur. Phys. J. Appl. Phys. **81**, 10101 (2018)
6. S.M. Taheri Otaqsara, Eur. Phys. J. Appl. Phys. **55**, 20403 (2011)
7. F. Yakuphanoglu, Y. Caglar, M. Caglar, S. Ilıcan, Eur. Phys. J. Appl. Phys. **58**, 30101 (2012)
8. S. Bayoud, M. Addou, K. Bahed, M. El Jouad, Z. Sofiani, M. Alaoui Lamrani, J.C. Bernéde, J. Ebothé, Phys. Scr. **T157**, 014045 (2013)
9. M. Alaoui Lamrani, M. El Jouad, M. Addou, T. El Habbani, N. Fellahi, K. Bahedi, M. Ebn Touhami, Z. Essaidi, Z. Sofiani, B. Sahraoui, A. Meghea, I. Rau, Spectrosc. Lett. **41**, 292 (2008)
10. A. Rherari, M. Addou, Z. Sofiani, M. El Jouad, M. Jbilou, M. Diani, A. Chahboun, J. Mater. Environ. Sci. **7**, 554 (2016)
11. A. Khataee, A. Karimi, M. Zarei, S.W. Joo, Ultrason. Sonochem. (2015)
12. V. Kumar, S. Som, V. Kumar, V. Kumar, O.M. Ntwaeaborwa, E. Coetsee, H.C. Swart, Chem. Eng. J. **255**, 541 (2014)
13. R. Zamiria, A.F. Lemosa, A. Rebloa, H.A. Ahangar, J.M.F. Ferreiraa, Ceram. Int. **40**, 523 (2014)
14. O. Maalej, M. El Jouad, N. Gaumer, S. Chaussedent, B. Boulard, M. Dammak Ben Ameur, M. Dammak Ben Tijani, J. Non-Cryst. Solids **420**, 48 (2015)
15. A. Monteil, S. Ghemid, S. Chaussedent, M. El Jouad, M.A. Couto dos Santos, Chem. Phys. Lett. **493**, 118 (2010)
16. C. Zhu, A. Monteil, M. EI Jouad, N. Gaumer, S. Chaussedent, J. Am. Ceram Soc. **93**, 1039 (2010)
17. C. Zhu, A. Monteil, M. El Jouad, N. Gaumer, S. Chaussedent, Opt. Lett. **34**, 3749 (2009)
18. A. Monteil, M. El Jouad, G. Alombert-Goget, S. Chaussedent, N. Gaumer, A. Chiasera, Y. Jestin, M. Ferrari, J. Non-Cryst. Solids **354**, 4719 (2008)
19. V. Mangalam, K. Pita, C. Couteau, Nanoscale Res. Lett. **11**, 73 (2016)
20. Y. Tan, Z. Fang, W. Chen, P. He, J. Alloys Compd. **509**, 6321 (2011)
21. S. López-Romero, M.J. Quiroz-Jiménez, M. Hipólito García, A. Aguilar-Castillo, World J. Condens. Matter. Phys. **4**, 227 (2014)
22. Y. Zhang, Y. Liu, L. Wu, E. Xie, J. Chen, J. Phys. D: Appl. Phys. **42**, 085106 (2009)
23. F. Touri, A. Sahari, A. Zouaoui, F. Deflorian, L. Guerbous, Surf. Rev. Lett. **27**, 1950114 (2020)
24. F. Otieno, M. Airo, R.M. Erasmus, A. Quandt, D.G. Billing, D. Wamwangi, Sci. Rep. **10**, 8557 (2020)
25. D. Dasha, N.R. Pandab, D. Sahua, Appl. Surf. Sci. **494**, 666 (2019)
26. U. Vinoditha, B.K. Sarojini, K.M. Sandeep, B. Narayana, S. R. Maidur, P.S. Patil, K.M. Balakrishna, Appl. Phys. A **125**, 436 (2019)
27. Y. Natsume, H. Sakata, T. Hirayama, H. Yanagita, Phys. Stat. Solidi A **148**, 485 (1995)
28. Y.M. Lu, X.P. Li, S.C. Su, P.J. Cao, F. Jia, S. Han, Y.X. Zeng, W.J. Liu, D.L. Zhu, J. Lumin. **152**, 254 (2014)
29. K. Wijeratne, V.A. Seneviratne, J. Bandara, Eur. Phys. J. Appl. Phys. **69**, 10403 (2015)
30. Y. Jin, Q. Cui, K. Wang, J. Hao, Q. Wang, J. Zhang, Appl. Phys. **109**, 553 (2011)
31. D. Dridi, Y. Litaiem, M. Karyaoui, R. Chtourou, Eur. Phys. J. Appl. Phys. **85**, 20401 (2019)
32. M.A. Thomas, W.W. Sun, J.B. Cui, Phys. Chem. C **116**, 6383 (2012)
33. H. Ftouhi, Z. El Jouad, M. Jbilou, M. Diani, M. Addou, Eur. Phys. J. Appl. Phys. **87**, 10301 (2019)
34. K. Bahedi, M. Addou, M. El Jouad, Z. Sofiani, M. Alaoui Lamrani, T. El Habbani, N. Fellahi, S. Bayoud, L. Dghoughi, B. Sahraoui, Z. Essaıdi, Appl. Surf. Sci. **255**, 4693 (2009)
35. A. Bougrine, M. Addou, A. El Hichou, A. Kachouane, J. Ebothé, M. Lamrani, L. Dghoughi, Phys. Chem. News **13**, 36 (2003)
36. R.R. Chamberlin, J.S. Skarman, J. Electrochem. Soc. **113**, 86 (1966)
37. A. El Hichou, M. Addou, J. Ebotheé, M. Troyon, J. Lumin. **113**, 183 (2005)
38. M. El Jouad, M. Alaoui Lamrani, Z. Sofiani, M. Addou, T. El Habbani, N. Fellahi, K. Bahedi, L. Dghoughi, A. Monteil, B. Sahraoui, S. Dabos, N. Gaumer, Opt. Mater. **31**, 1357 (2009)
39. O. Kamoun, A. Boukhachem, A. Yumak, P. Petkova, K. Boubaker, M. Amlouk, Mat. Sci. Semicon. Proc. **43**, 8 (2016)
40. A. Bouaoud, A. Rmili, F. Ouachtari, A. Louardi, T. Chtouki, B. Elidrissi, H. Erguig, Mater. Chem. Phys. **137**, 843e847 (2013)
41. B.D. Cullity, Elements of X-Ray Diffraction, 2nd edn. (Addison Wesley Publishing Co., Reading, MA, 1978)
42. Z. Sofiani, B. Derkowska, P. Dalasinski, M. Wojdyła, S. Dabos-Seignon, M. Alaoui Lamrani, L. Dghoughi, W. Bała, M. Addou, B. Sahraoui. Opt. Commun. **267**, 433 (2006)
43. M. Alaoui Lamrani, M. Addou, Z. Sofiani, B. Sahraoui, J. Ebothé, A. El Hichou, N. Fellahi, J.C. Bernède, R. Dounia, Opt. Commun. **277**, 196 (2007)
44. J. Wang, G. Du, Y. Zhang, B. Zhao, X. Yang, D. Liu, J. Cryst. Growth **263**, 269 (2004)
45. S.A. Studenikin, N. Golego, M. Cocivera, J. Appl. Phys. **84**, 4 (1998)
46. T. Minami, H. Nanto, S. Takata, J. Lumin. **2425**, 63 (1981)
47. K. Vanheusden, C.H. Seager, W.L. Warren, D.R. Tallant, J. A. Voigt, J. Appl. Phys. **68**, 403 (1996)

48. M. Wang, C. Huang, Z. Huang, W. Guo, J. Huang, H. He, H. Wang, Y. Cao, Q. Liu, J. Liang, Opt. Mater. **31**, 1502 (2009)
49. Q. Yu, T. Ai, L. Jiang, Y. Zhang, C. Li, X. Yuan, RSC Adv. **4**, 53946 (2014)
50. V. Kumar, V. Kumar, S. Som, M.M. Duvenhage, O.M. Ntwaeaborwa, H.C. Swart, Appl. Surf. Sci. **308**, 419 (2014)
51. P.M. Aneesh, M.K. Jayaraj, Bull. Mater. Sci. **33**, 227 (2010)
52. L. Castañeda, O.G. Morales-Saavedra, D.R. Acosta, A. Maldonado, M. de la L Olvera, Phys. Stat. Solidi A **203**, 1971 (2006)
53. J. Ebothe, W. Gruhn, A. Elhichou, I.V. Kityk, R. Dounia, M. Addou, Opt. Laser Technol. **36**, 173 (2004)

Cite this article as: Mohamed El Jouad, El Mehdi Bouabdalli, Samira Touhtouh, Mohammed Addou, Nadège Ollier, Bouchta Sahraoui, Red luminescence and UV light generation of europium doped zinc oxide thin films for optoelectronic applications, Eur. Phys. J. Appl. Phys. **91**, 10501 (2020)